

Monte Carlo simulation for internal radiation dosimetry based on the high resolution Visible Chinese Human

LIU Yang^{1,2} XIE Tianwu^{1,2} LIU Qian^{1,2,*}

¹*Britton Chance Center for Biomedical Photonics, Wuhan National Laboratory for Optoelectronics, Huazhong University of Science and Technology, Wuhan 430074, China*

²*Key Laboratory of Biomedical Photonics of Ministry of Education, College of Life Science and Technology, Huazhong University of Science and Technology, Wuhan 430074, China*

Abstract The internal radiation dose calculations based on Chinese models is important in nuclear medicine. Most of the existing models are based on the physical and anatomical data of Caucasian, whose anatomical structure and physiological parameters are quite different from the Chinese, may lead significant effect on internal radiation. Therefore, it is necessary to establish the model based on the Chinese ethnic characteristics, and applied to radiation dosimetry calculation. In this study, a voxel model was established based on the high resolution Visible Chinese Human (VCH). The transport procedure of photon and electron was simulated using the MCNPX Monte Carlo code. Absorbed fraction (AF) and specific absorbed fraction (SAF) were calculated and S-factors and mean absorbed doses for organs with ^{99m}Tc located in liver were also obtained. In comparison with those of VIP-Man and MIRD models, discrepancies were found to be correlated with the racial and anatomical differences in organ mass and inter-organ distance. The internal dosimetry data based on other models that were used to apply to Chinese adult population are replaced with Chinese specific data. The obtained results provide a reference for nuclear medicine, such as dose verification after surgery and potential radiation evaluation for radionuclides in preclinical research, etc.

Key words Internal radiation, AF, SAF, S-factor, Mean absorbed dose

1 Introduction

In nuclear medicine, internal sources of ionizing radiation are used for therapeutic or diagnosis purposes. The radiation doses delivered to the human body must be determined as precisely as possible. A computational approach to evaluate the potential dose utilizing an anthropomorphic model and a Monte Carlo code is an effective and convenient way in dosimetry research, because the experimental measurements are either time-consuming or dangerous in practice.

Computational models have been classified as: (a) mathematical-equation-based stylized models, in which the organs are described by planar, conical,

cylindrical, elliptical or spherical surfaces, and (b) voxel-based models, in which organs are defined from segmented medical images^[1]. The mathematical models were first designed by Fisher and Snyder^[2] from Oak Ridge National Laboratory (ORNL) in 1968 and were revised in 1978. They were adapted by the Medical Internal Radiation Dose (MIRD) Committee, the Society of Nuclear Medicine, USA as the MIRD-type model, and have been evolved into several improved and extended versions for dosimetry calculation^[3–8]. With the development of computer and medical imaging techniques, computational anthropomorphic models developed from successive X-ray CT, magnetic resonance imaging (MRI) and cryosectional color photographic images have been increasingly applied to Monte Carlo simulations in

Supported by National Natural Science Foundation of China (Grant No. 10875047 and Grant No. 30700214) and Program for New Century Excellent Talents in University (Grant No. NCET-10-0386)

* Corresponding author. *E-mail address:* qianliu@mail.hust.edu.cn

Received date: 2011-04-18

radiological science for precise representations of human anatomic structure and gradually replaced the stylized models. Since 1984 when Gibbs *et al.*^[9] and Williams *et al.*^[10] independently introduced the voxel-based models into radiation dosimetry, over 30 models have been developed, such as the VIP-Man, GSF series and the MAX/FAX couple^[1].

However, most of the existing stylized models were developed according to the data on the ICRP Reference Man^[11,12], which is based on the physical and anatomical data of Caucasian. Qiu R *et al.* established the Chinese mathematical phantom and compared with the ORNL phantoms^[13]. However, the stylized models facilitate the rapid dose calculation, but suffer from the loss of most anatomic details. The existing voxel-based models are also based on the medical images of Caucasian subjects^[1]. Characteristics such as the body size and composition have significant effect on dosimetry results for internal radiation, though they have little effect for external irradiation^[14]. Therefore, it is imperative to establish the race-specific voxel model to evaluate more accurate internal dosimetry for Chinese human.

In this study, a Visible Chinese Human (VCH) voxel model was developed using the high-quality cryosectional dataset based on the VCH project. Under the simulation conditions of MCNPX version 2.5, the transports of photons and electrons were simulated. Absorbed fraction (AF), specific absorbed fraction (SAF) were calculated and compared with those of VIP-Man and MIRD models. S-factors and mean absorbed dose were also calculated.

2 Materials and methods

2.1 The VCH phantom

The tomographic image set utilized to develop the VCH computational phantom was obtained by high-quality cryosectional color photographic scanning on an adult Chinese male cadaver, who was 166 cm tall and weighed 58 kg. Procedures in developing the VCH voxel model, including image acquisition, segmentation and 3D reconstruction, have been described in a previous paper^[15] and the model has been utilized in external dosimetry calculations. The original transaxial color photographic images used

in this work were of 5440×4080 pixels in a voxel size of 0.1 mm×0.1 mm×0.2 mm^[16]. Considering the huge demands on time and memory to store the datasets, which could be handled by computers available currently, the voxel size used in this dosimetry simulation was adapted to 2 mm×2 mm×2 mm, hence a 4000-times reduction of the data amount, with acceptable compromise on anatomical representation. Mass comparisons for major organs and tissues within the VCH model against VIP-Man and MIRD models are tabulated in Table 1^[16,17]. The MIRD model has been mentioned before and the VIP-Man model was segmented from transversal color photographic images from the Visible Human Project (VHP) and utilized it for multi-particle calculations by Xu *et al.*^[17].

Table 1 Masses (in units of g) of some organ and tissue of the VCH, VIP-Man and MIRD

Organ/Tissue	VCH	VIP-Man	MIRD
Adrenals	5.0	8.3	16.3
Bladder wall	47.4	41.4	47.6
Brain	1034.9	1574	1420
Esophagus	36.4	38.9	—
Gall bladder	8.3	12	10.5
Heart wall	253.2	398.7	316
Intestine	1470.4	2142.8	1862
Kidneys	194.1	335.4	299
Liver	1180.5	1937.9	1910
Lungs	456.8	910.5	1000
Pancreas	39.5	82.9	94.3
Spleen	211	244	183
Stomach wall	96	159.5	158
Testes	17.4	21	39.1
Thymus	24.4	11.2	20.9
Thyroid	18.9	27.6	20.7

2.2 Monte carlo simulation

The Monte Carlo method has been widely used in studies on transport of photons, electrons and neutrons^[18], and on radiological and nuclear simulations^[19,20] where physical experiments are either dangerous or unfeasible. The MCNPX implementation of the VCH computational model was on a lattice of 460 mm×260 mm×1792 mm consisting of 220×130×896 voxels. The surrounding medium of the body was defined as air. Organ elemental compositions and tissue densities used in the VCH model were obtained

from ICRU Report 44^[21] and ICRP Publication 89^[12]. Monoenergetic photons and electrons were generated from a photon source of 15 keV to 4 MeV and an electron source of 0.1–4MeV.

2.3 Mean absorbed dose calculation

The Medical Internal Radiation Dose (MIRD) schema is adopted for the calculation of the mean absorbed dose which can be simplified as the product of the cumulated activity and S-factor^[22]:

$$D_{(t,T)} = \sum_s \int_0^T A_{(s,\tau)} S_{(t \leftarrow s, \tau)} d\tau \quad (1)$$

where $D_{(t,T)}$, in unit of rad or Gy, is the mean absorbed dose for given target organ t by radiation source s over a time period of T ; $A_{(s,\tau)}$, in unit of $\mu\text{Ci}\cdot\text{h}$ or $\text{MBq}\cdot\text{s}$, is the time-dependent activity of the radiopharmaceutical in source s ; $S_{(t \leftarrow s, \tau)}$ is the S-factor, in $\text{Gy}\cdot\text{MBq}^{-1}\cdot\text{s}^{-1}$, and it depends on the characteristics of the radionuclide and the anatomic specific of the phantom, describing the mean dose rate to target organ for a radionuclide. For a specific radionuclide, the S-factor is given by:

$$\begin{aligned} S_{(t \leftarrow s)} &= \frac{1}{m_t} \sum_i E_i Y_i \varphi_{i(t \leftarrow s)} \\ &= \frac{1}{m_t} \sum_i \Delta_i \varphi_{i(t \leftarrow s)} = \sum_i \Delta_i \Phi_{i(t \leftarrow s)} \end{aligned} \quad (2)$$

where E_i is the energy of such a particle, Y_i is the average number of the i^{th} radiation type particles emitted from source region per nuclear transition, Δ_i is the mean energy emitted per nuclear transition in

$\text{g}\cdot\text{Gy}\cdot\text{Bq}^{-1}\cdot\text{s}^{-1}$, m_t is the mass of target organ t in grams; $\varphi_{i(t \leftarrow s)}$ is the absorbed fraction (AF), and $\Phi_{i(t \leftarrow s)}$ is specific absorbed fraction (SAF), at energy E_i in the target organ t for the i^{th} radiation type originating in the source organ s , with the AF describing the proportion of energy deposited in target organ and the SAF describing the mean absorbed fraction in a target organ, i.e. ratio of the absorbed fraction and target mass.

3 Results and discussion

3.1 Internal photon radiation in VCH

In the internal radiation dose calculation of VCH model, 29 organs were selected as internal sources. The photon AFs and SAFs for these organs were calculated, as showed in Fig.1. All the curves in Fig.1 present a steep descent in 15–100 keV, with a local minimum at 100 keV, indicating that more photons escape from the source regions as the energy increases. At photon energy of 0.1 MeV, the values begin to increase slightly to a maximum at 0.5 MeV, where they begin to decrease again. This is because of Compton scattering of the photons in 0.1 MeV and beyond. At photon energy region of 0.1–0.5 MeV, more recoil electrons and scattered photons are generated by Compton scattering, hence increased energy deposition with the energy. After the local maximums, the recoil electrons and scattered photons of higher energies are more likely to escape from an organ, resulting in gentle descent of the values.

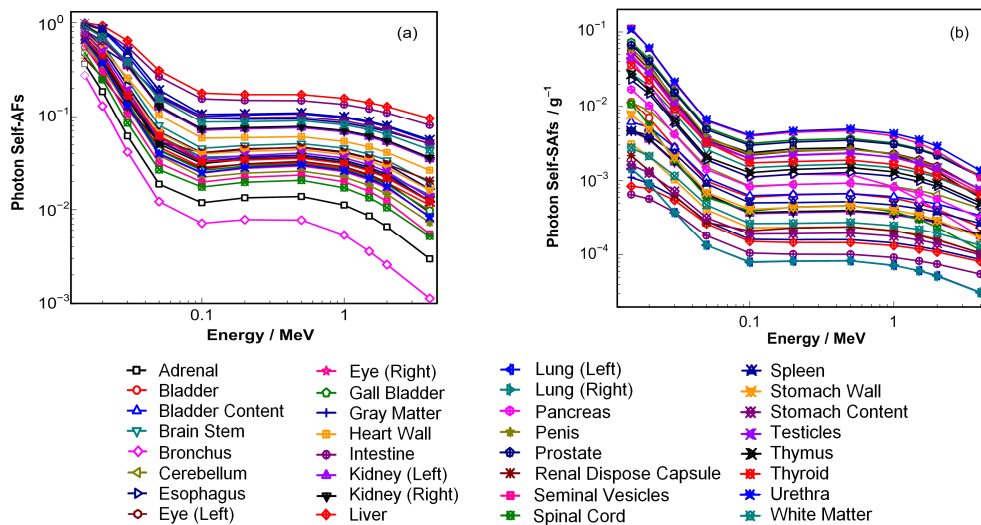


Fig.1 Photon AFs (a) and SAFs (b) for 29 organs in VCH.

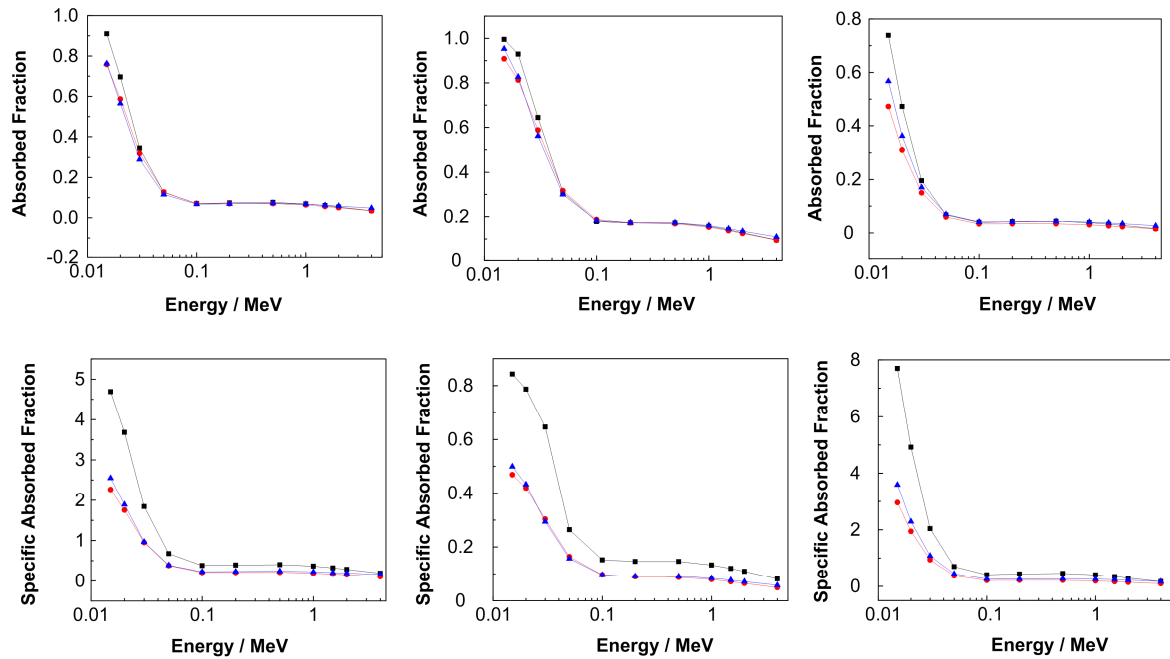


Fig.2 Photon AFs and SAFs for kidneys, liver and stomach wall in VHC(■), VIP-Man(●) and MIRD(▲).

Differences in organ AFs are mainly due to the discrepancies in physical properties of the organs, such as density, volume and shape. Both factors must be considered jointly. The bronchus, of the lowest density of $0.26 \text{ g}\cdot\text{cm}^{-3}$, which facilitates escape of the photons and electrons, has the smallest AF of all the organs in Fig.1a. The lung, having the same density as the bronchus, has a much higher AF due to its large volume of 1756.8 cm^3 , while the bronchus is of just 24.7 cm^3 . The intestine, of a larger volume (1413.9 cm^3) than the liver (1124.3 cm^3), has thin walls, which allows easy escape of the photons and electrons from it, hence a larger photon AFs for the liver than the intestine. The AF also depends on the particle energy. It does not differ much at photon energies of $<50 \text{ keV}$, due to poor penetration ability of the photons, but it increases with the energy. So, organs of higher density, larger volume and more uniform shape will have larger AFs than other organs at the same energy. The photon SAF is ratio of AF to the organ mass. For most cases, the SAFs are inversely proportional to the organ masses except for the organs of stomach (with thin walls), kidneys (its mass is distributed between two

organs), and bronchus and lungs (of low densities), as illustrated in Fig.1(b).

3.2 Photon radiation in different models

The AFs and SAFs of the organs were compared with different models. Fig.2 shows the AFs and SAFs for kidneys, liver and stomach wall in VHC, VIP-Man and MIRD models. In Figs.2a–2c, the AFs for the organs in three models do not differ greatly, and in Figs.2d–2f the SAFs for organs in the VHC model have the similar tendency with those in the VIP-Man and MIRD models, but they have larger values than those of the other two, especially for the liver. Considering the kidney masses are 197, 335.4, 299 g, the liver masses are 1180.5, 1937.9, 1910 g, and the stomach wall masses are 96, 497.7 and 158 g for the VHC, VIP-Man and MIRD models, respectively. It can be seen that racial difference in organ mass is reflected in the SAF results for the same source and target organs, and the SAFs for certain organs in different models are in inverse proportion to the organ masses.

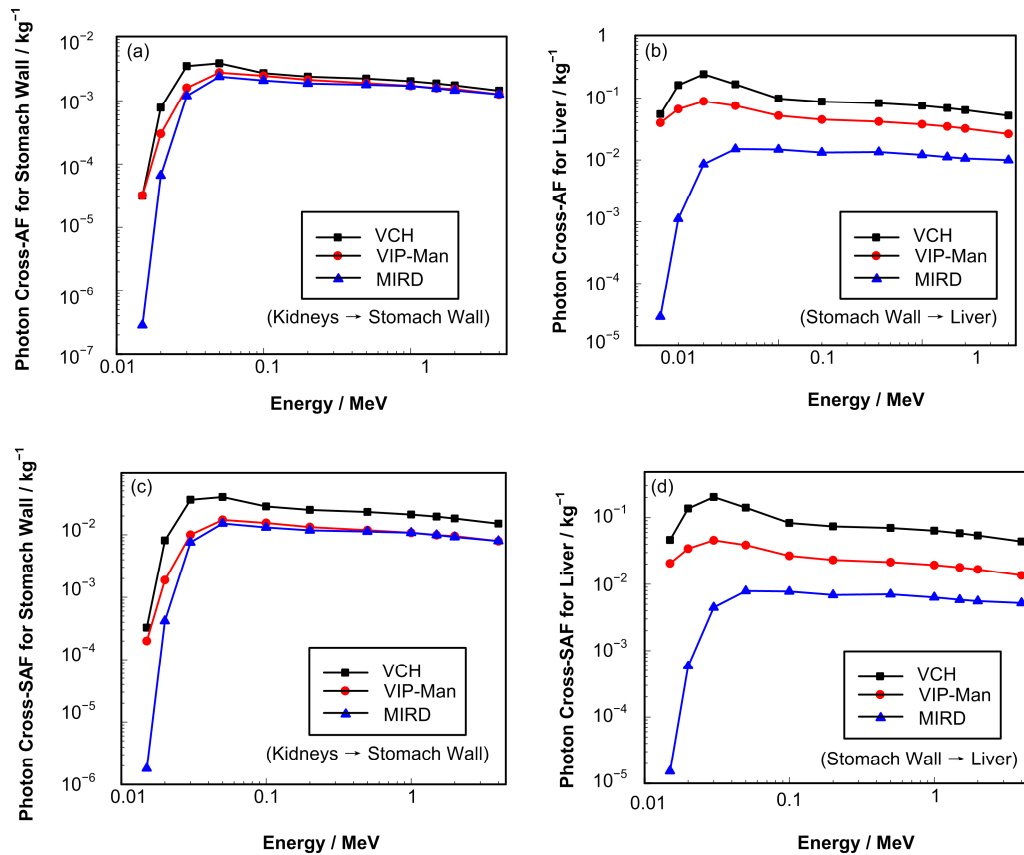


Fig.3 Photon (a) cross-AF (kidneys→stomach wall), (b) cross-AF (stomach wall→liver), and photon (c) cross-SAF (kidneys→stomach wall), (d) cross-SAF (stomach wall→liver): comparison with the results of VIP-Man and MIRD.

If the source and target organs are not identical, Figs.3a and 3b shows the comparisons of photon cross-AFs, i.e. kidneys→stomach wall and stomach wall→liver, in three models. The cross-AFs of kidneys→stomach wall of the VCH model have little discrepancies in comparison with the other two models in most cases. The cross-AFs of stomach wall→liver of the VCH model show similar tendency with the VIP-Man model, but it was about 90% higher than that of the VIP-Man model at 0.1 MeV. This may be due to the smaller mass of the stomach wall with a wall-like structure, which may facilitate the transport of the photon. The cross-AFs of stomach wall→liver of the VCH model was over 550% higher than that of MIRD model at 0.1 MeV. The differences of inter-organ distance from different models are the main reason of the difference of cross-AFs, especially for adjacent organs. In voxel models of VCH and VIP-Man, the

stomach is in contact with the liver, whereas there is a gap between the stomach and the liver in the MIRD model. It can be demonstrated that the anatomical realism in voxel model provided more realistic cross-AF values than the stylized models. As the kidneys are far from the stomach, the inter-organ distance has less influence on the cross-AF. Figs.3c and 3d show the comparisons of photon cross-SAFs of kidneys→stomach wall and stomach wall→liver in the three models. One sees that the VCH organs of smaller mass may lead to relative larger cross-SAFs in comparison with the other two models.

3.3 Potential risk to organs from internal electron radiation

Figure 4 shows the electron AFs and SAFs for 29 organs. Our findings are interesting. Electron AFs are always supposed to be 1 in MIRD schema, which

means that all the energy of electrons emitted from a source organ is assumed to be self-absorbed^[23,24]. However, Fig.4(a) demonstrates that electron energies is not always completely absorbed in the source organ.

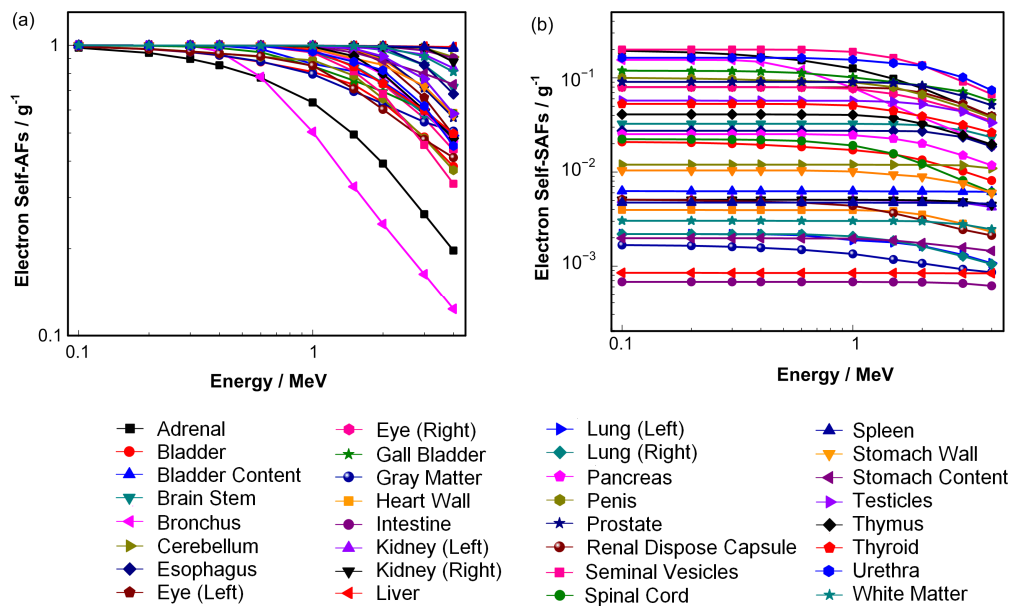


Fig.4 Electron self-AFs and self-SAFs for 29 organs of VCH.

The result suggested a new way to deal with internal electron dosimetry. Target organs can be classified into four categories according to the SAFs. The “highest target” is the target organ receiving the highest dose, which is usually the source organ itself. From radiotherapeutic point of view, a dose of a few tens of Sv is usually prescribed to the highest target. Compared to ICRP 60 recommended dose limits, a few tens of mSv of organ dose is critical to protect normal tissues from radiation. Therefore, organ having SAF less than 0.1% of that in highest target can be classified as “irrelevant organ”. When the SAF in a target organ is bigger than 1% of SAF in the highest target, it can be classified as the “neighbor target”. Finally, “nearby targets” are organs with SAF of 0.1%–1% of that in the highest target. In Table 2, the classifications for 29 source organs are given, by using SAFs for 4 MeV electrons (to be conservative). For example, if the electrons are emitted from stomach wall, dose to the stomach content and liver must be considered because they are neighbor targets receiving doses higher than 1% of the dose to stomach wall. Dose to artery, gall bladder and intestine, which are higher than 0.1% of the stomach wall, should be

All the AFs in Fig.4a decrease with increasing energies because higher energy electrons are more likely to escape from the source regions. The SAFs for organs are in similar trend, as shown in Fig.4b.

monitored for radiation protection. The neighbor targets and nearby targets for 29 source organs emitting electrons of 0.1–2 MeV are listed in Table 3. The results show that the surrounding organs receive considerable doses even for energies as low as 100 keV. It is convincing that electrons do affect the surrounding organs, and Tables 2 and 3 are of help to find the organs at risk.

3.4 S-factors and mean absorbed doses for organs

The photon and electron AFs for target organs were used to calculate S-factors for γ - and β -rays emitted from radionuclides that are commonly used in nuclear medicine. The decay data for ^{99m}Tc was acquired from the MIRD dose estimate report No.11^[25]. The AFs for each type of particles emitted from ^{99m}Tc were interpolated from monoenergetic photon and electron AF values. S-factors were obtained by summing photon and electron contributions. S-factors of ^{99m}Tc in the liver and target organs of the VCH, VIP-Man and MIRD models were calculated when liver was considered as the source organ, as listed in Table 4.

Organ dose can be calculated according to the S-factor and the radioactivity. For instance, 3.7×10^7 Bq

^{99m}Tc , which is used for liver imaging, was injected into the liver of VCH. According to the MIRD dose estimate report No.11, 85% of the injected ^{99m}Tc is uniformly deposited in the liver. The mean absorbed doses for the liver and other organs of VCH were

calculated according to the formula as mentioned before, and compared with those of VIP-Man and MIRD, assuming there is no biological removal, as listed in Table 4.

Table 2 Target organ classifications for 4 MeV electron emitters

Source organ (Highest target)	Neighbor target (>1% of highest target)	Nearby target (>0.1% of highest target)
Adrenal	Stomach wall	Stomach content
Bladder	Bladder content, Intestine	–
Bladder content	–	Bladder
Brain stem	–	Artery, Cerebellum, Gray matter, White matter
Bronchus	Esophagus, Thyroid	Artery, Skeleton
Cerebellum	Brain stem	–
Esophagus	–	Artery, Heart wall
Eye	–	–
Gall bladder	–	Liver
Gray matter	White matter	Eyes
Heart wall	Blood in Heart, Liver	–
Intestine	Artery	Pancreas
Kidneys	Renal dispose capsule, Spleen	–
Liver	–	–
Lungs	Artery, Bronchus, Skeleton	Blood in Heart, Esophagus, Heart wall, Muscle, RBM, Vein
Pancreas	Intestine	Artery, Stomach wall
Penis	Urethra	–
Prostate	Seminal vesicles	Urethra
Renal dispose capsule	Kidneys, Vein	Artery
Seminal vesicles	Bladder, Prostate	Bladder content
Spinal cord	Skeleton	–
Spleen	–	–
Stomach wall	Liver, Stomach content	Artery, Gall bladder, Intestine
Stomach content	Stomach wall	Artery, Skeleton
Testicles	–	–
Thymus	Blood in heart, Heart wall	Lungs
Thyroid	Artery	Esophagus
Urethra	Penis	–
White matter	Gray matter	–

S-factors and organ doses obtained from different phantoms show significant differences, owing to the variation in anatomic parameters (such as the volume, mass, shape, etc.) of different phantoms. The results

can be used to evaluate the potential radiation for a radionuclide in certain source organs of patients in preclinical research.

Table 3 Target organs which receive considerable doses (> 0.1%) for electron emitters with energies varied from 100 keV to 2 MeV

Source organ	100 keV	400 keV	600 keV	1 MeV	1.5 MeV	2 MeV
Adrenal	–	Renal dispose capsule				Renal dispose capsule, Stomach wall
Bladder	Bladder content				Bladder content, Intestine	
Bronchus	–	–	–	Esophagus, Thyroid		
Gall bladder	–	–	–	–	–	Liver
Gray matter	–	–	–	White matter		
Heart wall	–	–	–	–	Blood in heart	
Kidneys	–	–	–	Renal dispose capsule		
Lungs	–	–	Artery	Artery, Bronchus		
Pancreas	–	–	–	–	Artery	Artery, Intestine
Penis	–	–	–	–	–	Urethra
Renal dispose capsule	Kidneys		Kidneys, Vein			
Stomach wall	–	–	–	–	Stomach content	
Stomach content	–	–	–	Stomach wall		
Thymus	–	–	–	–	Heart wall	Blood in heart, Heart wall
Thyroid	–	–	–	–	Artery, Bronchus	
White matter	–	–	–	–	–	Gray matter

Table 4 Comparisons of S-factors and mean absorbed doses for organs with 1 mCi ^{99m}Tc distributed in liver with those of VIP-Man and MIRD

Organs	VCH		VIP-Man		MIRD Pamphlet No.11	
	S-factors / Gy·Bq ⁻¹ ·s ⁻¹	Doses / mGy	S-factors / Gy·Bq ⁻¹ ·s ⁻¹	Doses / mGy	S-factors / Gy·Bq ⁻¹ ·s ⁻¹	Doses / mGy
Adrenal	6.01×10 ⁻¹⁶	0.59	7.48×10 ⁻¹⁶	0.74	3.38×10 ⁻¹⁶	0.33
Kidneys	2.54×10 ⁻¹⁶	0.25	3.65×10 ⁻¹⁶	0.36	2.93×10 ⁻¹⁶	0.29
Liver	3.49×10 ⁻¹⁵	3.43	3.36×10 ⁻¹⁵	3.30	3.45×10 ⁻¹⁵	3.39
Lungs	7.77×10 ⁻¹⁶	0.76	2.80×10 ⁻¹⁶	0.28	1.88×10 ⁻¹⁶	0.18
Pancreas	3.38×10 ⁻¹⁶	0.33	5.50×10 ⁻¹⁶	0.54	3.15×10 ⁻¹⁶	0.31
Spleen	1.44×10 ⁻¹⁶	0.14	1.27×10 ⁻¹⁶	0.12	6.91×10 ⁻¹⁷	0.07
Stomach wall	4.59×10 ⁻¹⁶	0.45	4.98×10 ⁻¹⁶	0.49	1.43×10 ⁻¹⁶	0.14
Thyroid	8.57×10 ⁻¹⁷	0.08	5.06×10 ⁻¹⁷	0.05	1.13×10 ⁻¹⁷	0.01

4 Conclusion

A voxel model was established based on the high resolution Visible Chinese Human (VCH) in this study. Internal dosimetry simulations were performed based on this model. In comparisons with those of VIP-Man and MIRD models, discrepancies in dosimetry were found to be correlated with the racial and anatomical differences in organ mass and inter-organ distance. The internal dosimetry data based on other models that were used to apply to Chinese adult population are replaced with Chinese specific data. The obtained

results provide a reference for nuclear medicine, such as dose verification after surgery and potential radiation evaluation for radionuclides in preclinical research, etc.

References

- 1 Zaidi H, Xu X G. Annu Rev Biomed Eng, 2007, **9**: 471–500.
- 2 Fisher H L, Snyder W S. Oak Ridge National Laboratory Report No. ORNL-4168, 1967.
- 3 Snyder W S, Ford M R, Warner G G, *et al.* J Nucl Med, 1969, **10**: 5–52.

- 4 Snyder W S, Ford M R, Warner G G, *et al.* Medical Internal Radiation Dose (MIRD) Committee Pamphlet No.5 (revised), 1978.
- 5 Kramer R, Zankl M, William G, *et al.* GSF Report S-885, 1982.
- 6 Cristy M, Eckerman K F, *et al.* Oak Ridge National Laboratory Report No.ORNL/TM-8381 /V1-V7, 1987.
- 7 Stabin M G, Watson E E, Cristy M, *et al.* Oak Ridge National Laboratory Report ORNL /TM-1907, 1995.
- 8 Han E, Bolch W, Eckerman K, *et al.* Health Phys, 2006, **90**: 337–356.
- 9 Gibbs SJ, Pujol A Jr, Chen TS, *et al.* Oral Surg Oral Med O, 1984, **58**: 347–354.
- 10 Williams G, Zankl M, Abmayr W, *et al.* Phys. Med. Biol., 1986, **31**: 347–354.
- 11 International Commission on Radiological Protection. ICRP Publication 23 (Oxford: Pergamon), 1975.
- 12 International Commission on Radiological Protection. ICRP publication 89 (Oxford: Pergamon), 2002.
- 13 Qiu R, Li J L, Zhang Z, *et al.* Health Phys, 2008, **95**: 716–724.
- 14 International Atomic Energy Agency. Vienna: IAEA, 1998.
- 15 Zhang G Z, Luo Q M, Zeng S Q, *et al.* Health Phys, 2008, **94**: 118–125.
- 16 Li A A, Liu Q, Zeng S Q, *et al.* Chin Sci Bull, 2008, **53**: 1848–1854.
- 17 Xu X G, Chao T C, Bozkurt A, *et al.* Health Phys, 2000, **78**: 476–485.
- 18 Forster R A, Cox L J, Barrett R F, *et al.* Nucl Instr Meth Physics Res. B., 2004, **213**: 82–86.
- 19 Zhang G Z, Liu Q, Luo Q M. Phys Med Biol, 2007, **52**(24): 7367-7383.
- 20 Zhang G Z, Liu Q, Zeng S Q, *et al.* Phys Med Biol, 2008, **53**(14): 3697-3722.
- 21 International Commission Radiation Units and Measurements. ICRU Report44 (Bethesda, MD: ICRU), 1989.
- 22 Loevinger, R., Budinger, T.F., Watson, E.E. MIRD primer for absorbed dose calculations. Soc Nucl Med, ISBN 10 0932004253, 1991.
- 23 Petoussi-Hens N, Zankl M. Radiat Prot Dosim, 1998, **79**: 415–418.
- 24 Toohey R E, Stabin M G, Watson E E. Radiographics, 2000, **20**: 533–546.
- 25 Snyder W S, Ford M R, Warner G G, *et al.* Medical Internal Radiation Dose (MIRD) Committee Pamphlet No.11, 1975.